LAWRENCE
LIVERMORE
NATIONAL
LABORATORY

LLNL-SR-704084

A framework for WRF to WRF-IBM grid nesting to enable multiscale simulations

D. J. Wiersema, K. A. Lundquist, F. K. Chow

September 29, 2016

Disclaimer

This work performed under the auspices of the U.S. Department of Energy by Lawrence Livermore National Laboratory under Contract DE-AC52-07NA27344.

A framework for WRF to WRF-IBM grid nesting to enable multiscale simulations

DAVID JOHN WIERSEMA*

Civil and Environmental Engineering, University of California Berkeley, Berkeley, CA.
Lawrence Livermore National Laboratory, Livermore, CA.

KATHERINE A. LUNDQUIST
Lawrence Livermore National Laboratory, Livermore, CA.

FOTINI KATAPODES CHOW
Civil and Environmental Engineering, University of California Berkeley, Berkeley, CA.

ABSTRACT

With advances in computational power, mesoscale models, such as the Weather Research and Forecasting (WRF) model, are often pushed to higher resolutions. As the model's horizontal resolution is refined, the maximum resolved terrain slope will increase. Because WRF uses a terrain-following coordinate, this increase in resolved terrain slopes introduces additional grid skewness. At high resolutions and over complex terrain, this grid skewness can introduce large numerical errors that require methods, such as the immersed boundary method, to keep the model accurate and stable. Our implementation of the immersed boundary method in the WRF model, WRF-IBM, has proven effective at microscale simulations over complex terrain. WRF-IBM uses a non-conforming grid that extends beneath the model's terrain. Boundary conditions at the immersed boundary, the terrain, are enforced by introducing a body force term to the governing equations at points directly beneath the immersed boundary. Nesting between a WRF parent grid and a WRF-IBM child grid requires a new framework for initialization and forcing of the child WRF-IBM grid. This framework will enable concurrent multi-scale simulations within the WRF model, improving the accuracy of high-resolution simulations and enabling simulations across a wide range of scales.

1. Introduction

The Weather Research and Forecasting (WRF) model is an ideal starting point for developing a model capable of multi-scale atmospheric simulations. The WRF model, detailed in section 2, has a sizeable user base that spans both operational forecasting and research applications. With the advancement of computational resources, users of the WRF model have pushed the model to increasingly fine resolutions approaching the micro-scale, at less than 1 km. Many challenges exist for atmospheric simulations that span a wide range of spatial scales. These challenges include, but are not limited to, the difficulties traversing the "terra incognita" (Wyngaard 2004), restricted applicability of meso-scale physics parameterizations to the micro-scale, complications due to complex terrain at fine resolutions (Lundquist et al. 2012), and the absence of an atmospheric model capable of concurrently simulating both the meso-scale and micro-scale. This paper describes the ongoing development of the WRF model for use in multi-scale simulations.

Our solution to the issue of complex terrain is the addition of an immersed bounadry method (IBM) to the WRF model. This modified version of the model, called WRF-IBM, is detailed in section 4. WRF-IBM is necessary for micro-scale simulations since the maximum resolved terrain slope increases as horizontal resolution is refined, which results in grid distortion and numerical errors. WRF-IBM eliminates the numerical errors associated with grid distortion and enables the model to run over complex terrain, such as mountainous or urban environments.

Because of differences in the grid when using the immersed boundary method, a WRF domain cannot currently downscale information to a WRF-IBM domain. In order to nest a WRF-IBM domain within a WRF parent domain, several significant modifications must be made. First, vertial interpolation must be added for nesting between domains that do not have idential vertical grids. Details of the vertical grid nesting procedure that has been added into the WRF model are included in section 3.

Next, the nesting framework must be modified to allow for a nested domain to have a different model bottom than its parent domain. This is necessary beause the IBM requires additional vertical grid levels that extend below the model topography. The first step of this modification, replacing the coordinate used for vertical interpolation during nesting, is detailed in section 5. Testing of the modifications is detailed in section 6 and results are included in section 7.

*Corresponding author address: Civil and Environmental Engineering, University of California Berkeley, Mail Code 1710, Berkeley, CA 94709.
E-mail: wiersema@berkeley.edu

Ongoing and future work required to enable nesting between WRF and WRF-IBM domains is detailed in section 8.

2. The Weather Research and Forecasting model

The Weather Research and Forecasting (WRF) model is an open-source, community-developed, meso-scale, numerical weather prediction model (Skamarock et al. 2008). WRF has the capability of running as a large eddy simulation model with a variety of turbulence closure options (Moeng et al. 2007). The model contains two dynamics "cores", each of which uses different numerical methods, governing equations, and physics parameterizations. These two cores are the Nonhydrostatic Mesoscale Model (NMM) core and the Advance Research WRF (ARW) core. The NMM core is typically used for operational forecasting, while the ARW core is primarily used for research, teaching, and other specialized applications. The model modifications and simulation results presented in this paper are from the ARW core of WRF version 3.6.1.

WRF-ARW is fully compressible and non-hydrostatic, although it can be run with a hydrostatic option. Time integration is accomplished using a 3rd order Runge-Kutta scheme with a small time step to handle acoustic and gravity-wave modes. Spatial discretization for horizontal and vertical advection is performed with one of several options that range from 2nd to 6th order. WRF uses Arakawa C-grid staggering. The model's vertical coordinate, denoted by η, is terrain-following and based upon hydrostatic-pressure. Figure 1 shows a slice through an example WRF grid.

When calculating horizontal and vertical diffusion using the ARW dynamical core of the WRF model, coordinate metric terms are included to help reduce numerical error due to grid deformation caused by the terrain-following vertical coordinate (Skamarock et al. 2008). Despite these metric terms, the numerical errors can frequently become too great for the model to remain stable when running over complex terrain. This problem is especially common when running at high horizontal resolutions, since the maximum resolved terrain slope increases when horizontal grid resolution is refined.

Downscaling in WRF is performed through grid nesting, where a coarse-resolution "parent" domain provides boundary conditions for a "child" domain that is a high-resolution subset of the parent. The model supports both one-way grid nesting and two-way grid nesting. In two-way grid nesting, the child's solution provides "feedback" and nudges the parent's solution towards the child's solution at grid-cells where the two domains overlap. Concurrent nested simulations with different vertical grids are not possible and every nested domain must have the same number and placement of vertical grid levels as the parent domain. This is especially troubling for large eddy simulations (LES) where the grid aspect ratio can heavily influence the model's accuracy.

3. Vertical grid nesting in WRF

Vertical refinement during grid nesting can provide many advantages to a WRF simulation. When running WRF at LES-sales with a Smagorinsky or NBA1 closure model, a grid aspect ratio $\left(\frac{\Delta x}{\Delta z}\right)$ of less than 4.0 is necessary for accurate and rapid development of tubulent features in nested domains (Mirocha et al. 2013). Vertical grid nesting provides control over the number and placement of vertical grid levels, enabling the modeler to have full control over the grid aspect ratio of both the parent and nested domains. Another advantage of vertical nesting is the ability to use high vertical resolution in only the domains where it is necessary, which can save considerable computational time by greatly reducing the number of vertical levels of the parent domains.

a. Serial vertical nesting with ndown

Ndown was introduced with the public release of WRF version 3.2 and enables a nested domain to have additional vertical grid levels compared to its parent domains. With ndown, the nested domain's vertical grid levels are set by inserting $n-1$ levels between those of the parent domain, where n is an integer ratio of the number of vertical levels in the two domains.

Initialization and boundary condition updates for a domain nested with ndown require parent domain history files. As a result, the parent and nested domains must be run sequentially and cannot be concurrently simulated. Once the parent domain history file is available, the nested domain can be initialized and run using ndown and WRF. The nest's lateral boundaries are updated at each time stored within the parent's history file. The dependence on a history file makes two-way nesting impossible and presents issues for high-resolution simulations where it would be infeasible to store the number of timesteps required to accurately translate turbulent flow features to the nested domain from the parent domain (Michioka and Chow 2008).

The vertical interpolation in ndown is performed using cubic monotonic splines with Hermite polynomials and a vertical coordinate based on log-pressure height calculated from the hydrostatic component of pressure at the domain top, the domain's sigma levels, and a reference surface pressure (Moustaoui et al. 2009). A description of the vertical coordinate is included below in equation 1.

$$\zeta = -6.7 \cdot log\left(\frac{\left(10^5 - p_{ht}\right)\eta + p_{ht}}{10^5}\right) \qquad (1)$$

b. Concurrent vertical nesting

Recently, the WRF public release has included the ability to concurrently run nested domains with different vertical grids (Daniels et al. 2016). This new nesting functionality uses the same vertical interpolation scheme and vertical coordinate formulation as ndown. Vertical interpolation is performed after horizontal interpolation. Include-files, *nest_forcedown_interp_vert.inc* and *nest_interpdown_interp_vert.inc* are created during compile-time and contain calls to subroutines responsible for vertical interpolation of variables that are marked in the registry to be downscaled for initialization of the nest or for use in forcing the nest's lateral boundaries during integration.

With concurrent vertical grid nesting, updated parent information is passed to the child after every parent timestep, removing the dependancy on history output that often restricts the forcing update frequency when using ndown. Concurrent vertical grid nesting also includes the ability to have a child domain with a vertical grid that is independent of the parent domain vertical grid. This enables the modeler to optionally specify grid levels for each domain without ndown's requirement that a nested domain must have a refined version of the parent vertical grid.

4. The immersed boundary method

WRF-IBM is a version of the WRF model that has been modified to use an immersed boundary method (IBM), which enables simulations over complex terrain, such as mountainous or urban environments. The first immersed boundary method was developed in 1972 by Charles Peskin for the simulation of blood flow through the heart (Peskin 1972). IBMs are especially useful for simulation of fluid flow over complex terrain or flexible boundaries since the method provides a convenient way to determine the force exerted on the boundary by the fluid.

WRF-IBM utilizes a non-conforming structured grid, where the grid is independent of the immersed boundary, IB. An example grid is shown in figure 2. Boundary conditions are imposed at the immersed boundary through the addition of a body force term in the conservation equations for momentum and scalars, equations 2 and 3.

$$\partial_t V + V \cdot \nabla V = -\alpha \nabla p + \nu \nabla^2 V + g + F_B \tag{2}$$

$$\partial_t \phi + V \cdot \nabla \phi = \nu_t \nabla^2 \phi + F_\phi + F_B \tag{3}$$

Here V is the velocity vector, ϕ a scalar quantity, α the specific volume, F_B the body force term, and F_ϕ is the additional scalar forcing (Lundquist 2010; Lundquist et al. 2010, 2012). The body force term modifies the governing equations near the immersed boundary and assumes a value of zero when away from the immersed boundary. Additional forcing is applied at computational nodes beneath and adjacent to the immersed boundary to maintain the desired boundary condition. These nodes where additional forcing is applied are hereon referred to as "ghost-points".

To determine the magnitude of a ghost-point, the point's location is reflected across the immersed boundary, creating what will be referred to as an image-point. The image-point's magnitude is set by an interpolation scheme using nearby points within the fluid domain and, depending on the type of boundary condition being applied, the value at the boundary. The ghost-point's value is then determined using equation 4 for a Dirichlet boundary condition or equation 5 for a Neumann boundary condition.

$$\phi_G = 2\phi_\Omega - \phi_I \tag{4}$$

$$\phi_G = \phi_I - \overline{GI}\frac{\partial \phi}{\partial n}|_\Omega \tag{5}$$

In equations 4 and 5, ϕ_G is the ghost-point's value, ϕ_I is the image-point's value, and ϕ_Ω is the value at the immersed boundary. $\overline{GI}$ is the distance between the ghost and image points and $\frac{\partial \phi}{\partial n}|_\Omega$ is the gradient value assigned at the immersed boundary for a Neumann boundary condition.

WRF-IBM has been extensively validated for idealized test cases (Lundquist 2010; Lundquist et al. 2010, 2012). The model has already been used to simulate several micro-scale systems such as urban dispersion (Lundquist et al. 2012) and the development of thermally driven slope-flows (Arthur et al. 2016). Model development is continuing and includes the adaptation of surface layer schemes, such as a log-law bottom boundary condition, for use with the immersed boundary method (CITE JINGYI?).

5. WRF to WRF-IBM nesting (ongoing work)

While WRF-IBM has opened the door for micro-scale simulations over complex terrain to be performed using the WRF model, the immersed boundary method does not provide additional functionality to meso-scale simulations where the relatively smooth terrain does not cause a detrimental amount of grid distortion. Additionally, many of the WRF parameterization schemes require a significant amount of updating for compatibility with the immersed boundary method. As a result, the WRF-IBM model is currently uniquely suited for application at micro-scale resolutions only.

An ideal setup for multi-scale simulations using WRF would consist of a series of concurrently nested domains with meso-scale domains using the WRF model with terrain-following coordinates and micro-scale domains using the WRF-IBM model. This approach requires a framework for data to be interpolated from a parent domain using WRF's traditional terrain-following coordinate to a child domain using the immersed boundary method.

The WRF to WRF-IBM nesting framework discussed below is currently under development. Several major updates to various parts of the WRF model are required. An input file is necessary to initialize the grid of the nested WRF-IBM domain. Creation of this input file required updating the two input generation programs used by WRF. The input generation program used for real data cases is being modified to set the additional variables required by WRF-IBM. The input generation program used for idealized data cases has previously been modified for use with WRF-IBM however this program has now been modified to produce multiple input files, one for the parent domain and one for each nested domain.

Next, the vertical interpolation procedure from vertical grid nesting was modified for use with a parent and nest with different model bottoms. Because the immersed boundary method requires ghost points beneath the immersed boundary, the nested domain has a bottom boundary that sits several grid points beneath the bottom of the terrain whereas the parent domain's bottom boundary is coincident with the terrain surface. The vertical coordinate used for vertical interpolation was calculated using the model's η-levels, which vary from 1.0 at the model bottom to 0.0 at the model top and are set using equation 6 where p_h is the hydrostatic component of pressure and p_{hb} and p_{ht} are values at the model bottom and model top.

$$\eta = \frac{p_h - p_{ht}}{p_{hb} - p_{ht}} \tag{6}$$

Because the model bottom is no longer shared between nested domains, the vertical coordinate used for vertical interpolation requires a new formulation to be comparable between parent and child domains. The updated vertical coordinate described by equation 7 is calculated using a reference surface pressure of 10^5 Pa, an atmospheric scale height of 6.7 km, the hydrostatic component of pressure at the model top p_{ht}, the hydrostatic component of pressure at the vertical grid level being analyzed p_h, and p_{h_min} and p_{h_max} which are the minimum and maximum hydrostatic components of pressure from the union of parent and nest domains. p_h, the hydrostatic component of pressure, is calculated according to equation 8 using p_{hb} and p_{ht} as well as the domain's η-levels.

$$\zeta = -6.7 \cdot log\left(\frac{\left(10^5 - p_{ht}\right) \cdot \frac{p_h - p_{h\_min}}{p_{h\_max} - p_{h\_min}} + p_{ht}}{10^5}\right) \tag{7}$$

$$p_h = \eta\left(p_{hb} - p_{ht}\right) + p_{ht} \tag{8}$$

The original vertical coordinate defined in equation 1 and used by the original vertical grid nesting approach and ndown, depends only on the hydrostatic component of pressure at the domain top, p_{ht}, and the domain η-levels, both of which are horizontally invariant. For the updated vertical coordinate, differences in p_{hb} between the parent and child cause horizontal variation. As a result, the vertical coordinate is calculated for each column and passed into the vertical grid nesting subroutines as a three-dimensional array.

For situations where the parent and child domains have identical p_{hb} and p_{ht}, then $p_{h\_min} = p_{hb}$ and $p_{h\_max} = p_{ht}$, which results in the updated vertical coordinate simplifying and being equivalent to the original vertical coordinate. To validate the implementation of the updated coordinate, several idealized test cases were performed as described in section 6.

6. Validation of updated vertical nesting coordinate

Three test cases were performed to evaluate the updated vertical coordinate used by concurrent vertical grid nesting. Section 6a describes the setup for simulations initialized with quiescent conditions over a flat plate. This setup enables a comparison of simulations performed with and without the updated vertical coordinate and provides an indication of whether the updated coordinate causes model error, which would appear as the development of spurious flow. Section 6b describes the setup for simulations of moist and stably stratified flow over a flat plate. Section 6c describes the setup for simulations of dry and neutrally-stratified flow over a gaussian hill.

a. Quiescent flat plate

Simulations are initialized as quiescent, $\overline{V} = (u, v, w) = 0.0$, with a horizontally invariant, dry, and neutrally stratified vertical profile with potential temperature of 300 K. Lateral boundary conditions are periodic for the parent domain and nested for the child domain. Shortwave and longwave radiation physics parameterizations are not enabled. No land surface parameterization or surface layer scheme is applied and there is no surface heat flux. Horizontal and vertical mixing coefficients are held constant at 1.0 m s^{-2}.

Both the parent and child domains are dimensioned with 31 points in both the east-west and south north directions. There are 40 grid points in the vertical dimension for the parent domain and 118 for the child domain. The vertical grid of the child is set by inserting two new levels between each set of parent levels. This results in a refined version of the parent grid where every third vertical level of the child is aligned with a parent level. Horizontal resolution is 99 meters for the parent and 33 meters for the child. The model top is located at 4 km and the flat terrain at 0 meters. Rayleigh damping with a coefficient of 0.1 is applied to the top 500 meters of each domain.

b. Flow over a flat plate

The grid configuration for the simulations of flow over a flat plate is identical to that used for the quiescent simulations described in section 6a however the initial conditions are modified as follows. Both domains are initialized with an east-west velocity of 10.0 m s^{-1} at all points, vapor mixing ratio of 5.0 g kg^{-1} below 1 km ASL and 0.5 g kg^{-1} above 1 km ASL, potential temperature of 300 K below 1 km, and a lapse rate of -10 K km^{-1} upwards of 1 km ASL.

c. Flow over a gaussian hill

Similar to the prior two cases, the simulations for flow over a gaussian hill are performed with two nested domains with periodic lateral boundary conditions on the parent. Horizontal resolution is 99 meters for the parent and 33 meters for the child. The model top is located at 4 km and the ground topography is set following equation 9 where n_x and n_y are the number of grid points in the east-west and north-south dimensions and Δ_x and Δ_y are the horizontal grid resolutions.

$$H_{i,j} = \frac{125}{1 + \left(\frac{\frac{-n_x\Delta_x}{2} + i\Delta_x}{250}\right)^2 + \left(\frac{\frac{-n_y\Delta_y}{2} + j\Delta_y}{250}\right)^2} \qquad (9)$$

Both the parent and child have 91 grid points in the south-north and east-west dimensions. The parent has 40 vertical grid levels and the child's vertical grid has 118 levels with every third level coinciding with a parent level.

7. Results of the updated vertical nesting coordinate

a. Quiescent flat plate

Analysis of the vertical velocities that developed in the quiescent simulations show that the updated vertical coordinate causes slightly higher velocities, and thus model error. Figure 6 shows that the magnitude of these velocity differences is small, on the order of 10^{-3} m s^{-1}, and grows over the first three hours of simulation but remains constant thereafter. This indicates that the updated vertical coordinate is not detrimentally effecting the stability of the model.

b. Flow over a flat plate

Figures 7 and 8 show contours and vertical profiles of U-velocity for the test-case of flow over a flat plate. There is excellent agreement between the two simulations. Differences in the U-velocities between the two simulations are shown in figure 9. The maximum differences in U-velocity are on the order of 10^{-3} m s^{-1}, which is the same magnitude as the errors seen earlier in the quiescent test-case.

c. Flow over a gaussian hill

There is good agreement shown in the comparisons of the simulations of flow over a gaussian hill performed with and without the updated vertical coordinate for nesting. Figures 11 and 12 show differences of U and W velocities on the order of 10^{-3} m s^{-1} after six hours of simulation. This is once again comparable to the errors seen in the quiescent flat plate test-case.

8. Ongoing and future work

A significant amount of additional model development is still required to develop a framework for nesting with a WRF parent domain and WRF-IBM child domain. One necessary development is the addition of lateral boundary conditions for grid-points that are beneath the immersed boundary and along a domain edge. These added boundary conditions will help constrain the model solution beneath the immersed boundary.

Another requirement is the development of a treatment for perturbation geopotential at the immersed boundary. In a typical WRF simulation, the perturbation geopotential maintains a value of zero at the model bottom. When nesting a WRF-IBM domain within a WRF parent domain, the bottom of the domains do not align. This results in a discontinuity where perturbation geopotential has a value of zero at the bottom of the parent domain but the corresponding level on the nested domain may have nonzero values.

9. Conclusions

Developing the WRF model for multi-scale modeling holds many challenges, both predictable and unforseen. Micro-scale modeling in WRF is currently possible using an immersed boundary method. The recently released vertical grid nesting capability provides additional control of grids in nested simulations, which is necessary for micro-scale modeling. A modified version of the vertical grid nesting functionality is a key component for developing a framework to enable nesting with a WRF parent domain and a WRF-IBM child domain. This framework will provide the capability to nest WRF and WRF-IBM domains, bridging the meso-scale and micro-scale and enabling multi-scale atmospheric simulations within the WRF model.

Acknowledgments. Funding for this research was provided by Lawrence Livermore National Laboratory LDRD 14-ERD-024. This work was performed under the auspices of the U.S. Department of Energy by Lawrence Livermore National Laboratory under Contract DE-AC52-07NA27344.

References

Arthur, R., K. Lundquist, J. Mirocha, S. Hoch, and F. Chow, 2016: High-resolution simulations of downslope flows over complex terrain using wrf-ibm. *17th Conference on Mountain Meteorology*, Burlington, VT, American Meteorological Society.

Daniels, M., K. Lundquist, J. Mirocha, D. Wiersema, and F. Chow, 2016: A new vertical grid nesting capability in the weather research and forecasting (wrf) model. *Mon. Wea. Rev.*, manuscript accepted for publication.

Lundquist, K., 2010: Immersed boundary methods for high-resolution simulation of atmospheric boundary-layer flow over complex terrain. Ph.D. thesis, Univeristy of California, Berkeley, 159 pp.

Lundquist, K., F. Chow, and J. Lundquist, 2010: An immersed boundary method for the weather research and forecasting model. *Mon. Wea. Rev.*, **138**, 796–817.

Lundquist, K., F. Chow, and J. Lundquist, 2012: An immersed boundary method enabling large-eddy simulations of complex terrain in the wrf model. *Mon. Wea. Rev.*, **140 (12)**, 3936–3955, doi:10.1175/MWR-D-11-00311.1.

Michioka, T., and F. Chow, 2008: High-resolution large-eddy simulations of scalar transport in atmospheric boundary layer flow over complex terrain. *J. Appl. Meteor. Climatol.*, **47**, 3150–3169, doi:10.1175/2008JAMC1941.1.

Mirocha, J., G. Kirkil, E. Bou-Zeid, F. Chow, and B. Kosović, 2013: Transition and equilibrium of neutral atmospheric boundary layer flow in one-way nested large-eddy simulations using the weather research and forecasting model. *Mon. Wea. Rev.*, **141**, 918–940, doi:10.1175/MWR-D-11-00263.1.

Moeng, C.-H., J. Dudhia, J. Klemp, and P. Sullivan, 2007: Examining two-way grid nesting for large eddy simulation of the pbl using the wrf model. *Mon. Wea. Rev.*, **135**, 2295–2311, doi:10.1175/MWR3406.1.

Moustaoui, M., A. Mahalov, J. Dudhia, and D. Gill, 2009: Nesting in wrf with vertical grid refinement and implicit relaxation. *WRF Users' Workshop 2009*, Boulder, CO, National Center for Atmospheric Research.

Peskin, C. S., 1972: Flow patterns around heart valves: A digital computer method for solving the equations of motion. Ph.D. thesis, Albert Einstein College of Medicine, 211 pp., [Available from: http://www.umi.com/hp/Products/DisExpress.html, order no. 7230378].

Skamarock, W. C., and Coauthors, 2008: A description of the advanced research wrf version 3. NCAR Technical Note TN-475+STR, NCAR, 125 pp. [Available online at http://www2.mmm.ucar.edu/wrf/users/docs/arw_v3.pdf.].

Wyngaard, J. C., 2004: Toward numerical modeling in the "terra incognita". *J. Atmos. Sci.*, **61 (14)**, 1816–1826.

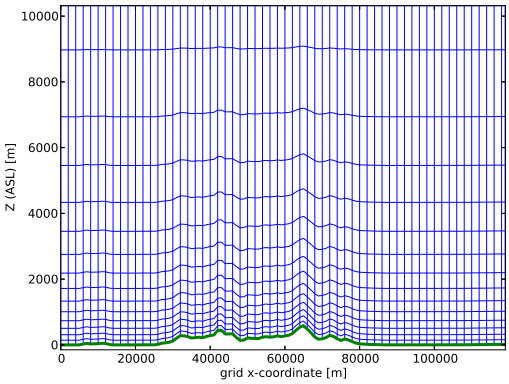

FIG. 1. Vertical slice through an example of a WRF grid.

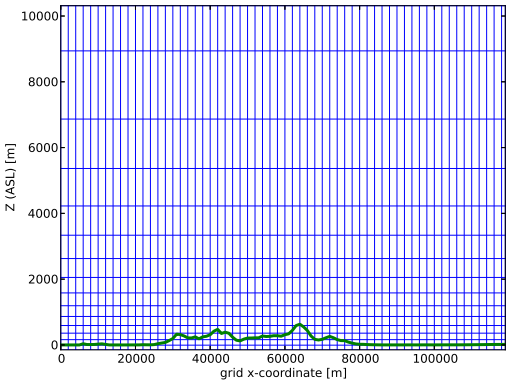

FIG. 2. Vertical slice through an example of a WRF-IBM grid.

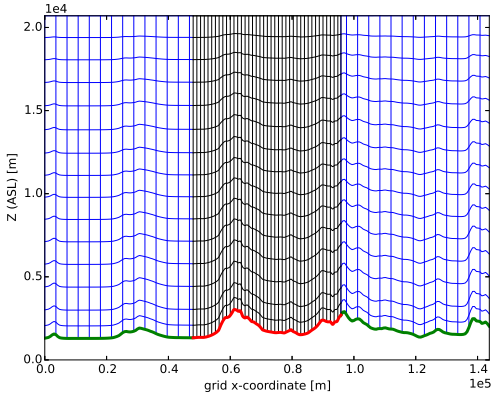

FIG. 3. Vertical slice through an example of nested domains in WRF. Every sixth grid-line is displayed.

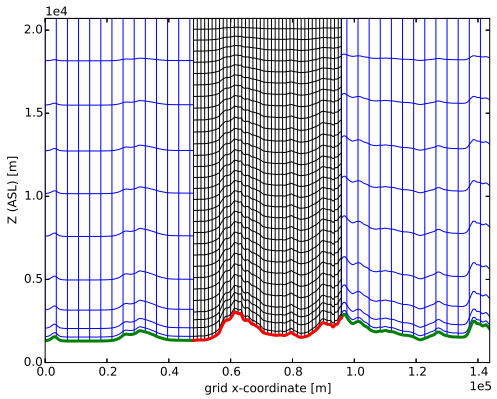

FIG. 4. Vertical slice through an example of nested domains in WRF with vertical grid nesting. Every sixth grid-line is displayed.

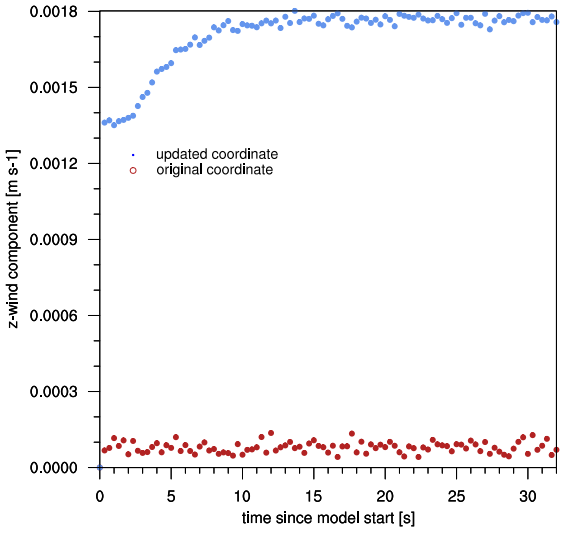

FIG. 6. Timeseries of W velocities for the quiescent test-case. Time-0 corresponds to the model start time.

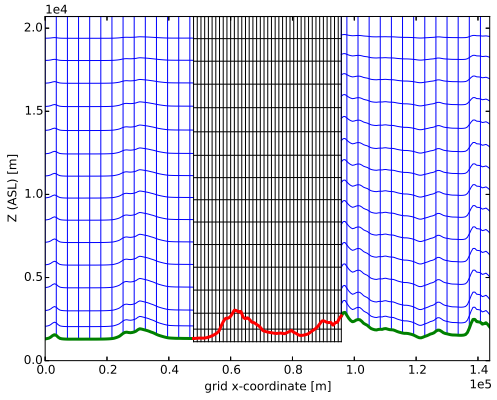

FIG. 5. Vertical slice through an example of a WRF-IBM domain nested within a WRF domain with terrain-following coordinates. Every sixth grid-line is displayed.

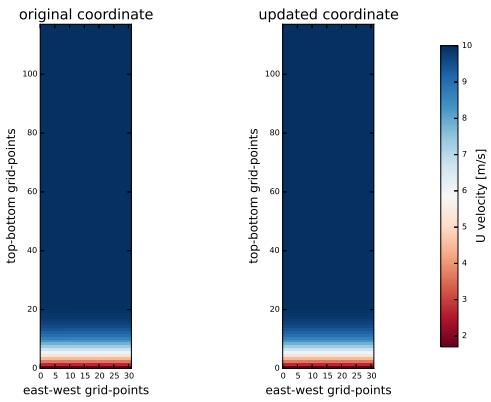

FIG. 7. East-west vertical slice showing U-velocity on the nested domain for the test-case of flow over a flat plate after 6 hours of simulation.

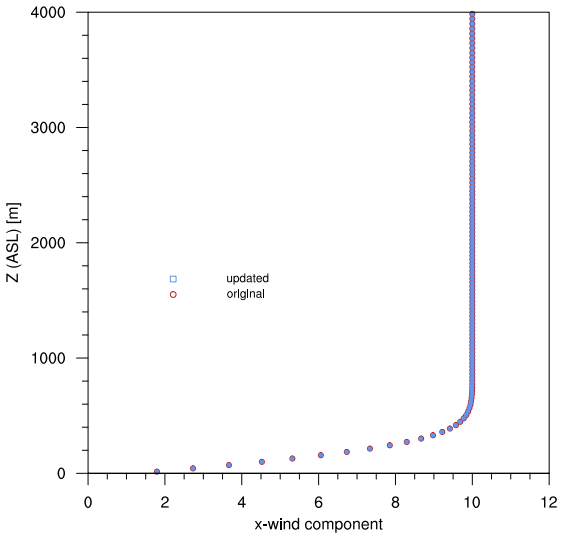

FIG. 8. Vertical profiles of U-velocity on the midpoint of the nested domain for the test-case of flow over a flat plate after 6 hours of simulation.

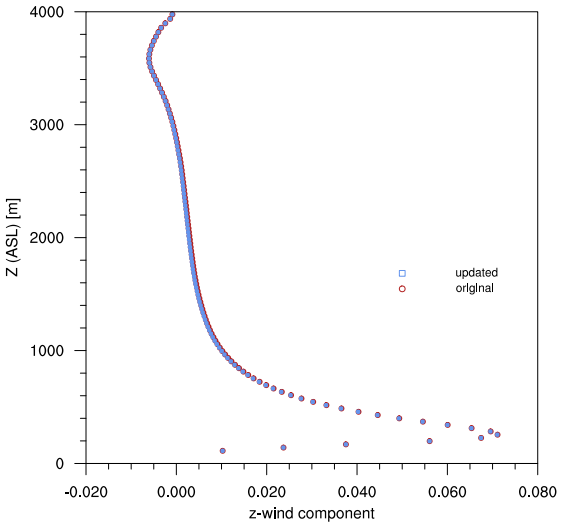

FIG. 10. Vertical profiles of W-velocity at the apex of the hill on the nested domain for the test-case of flow over a gaussian hill after 6 hours of simulation.

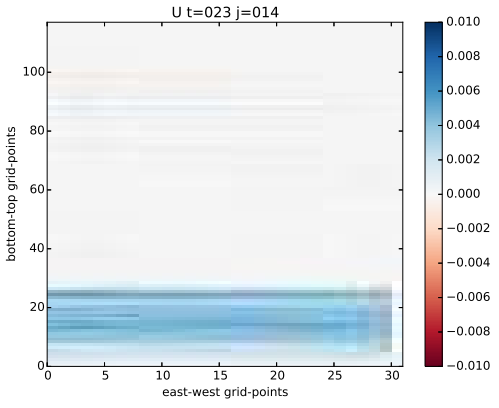

FIG. 9. East-west vertical slice showing the differences (original minus updated) in U-velocities between the original and updated vertical coordinate for the test-case of flow over a flat plate after 6 hours of simulation.

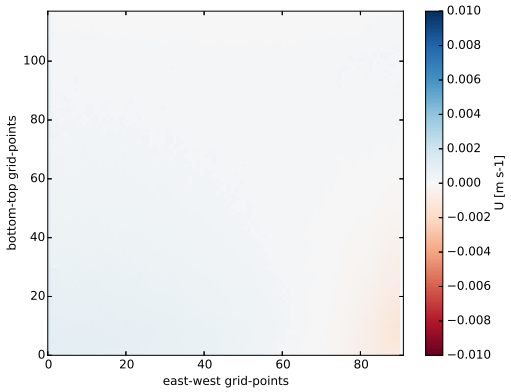

FIG. 11. Difference between U-velocities (original minus updated vertical coordinate) for the test-case of flow over a gaussian hill after 6 hours of simulation.

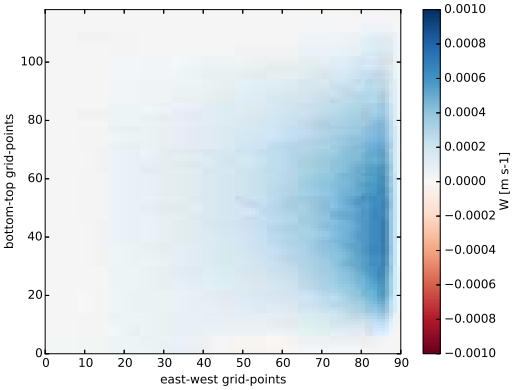

FIG. 12. Difference between W-velocities (original minus updated vertical coordinate) for the test-case of flow over a gaussian hill after 6 hours of simulation.